JOURNAL OF GEOPHYSICAL RESEARCH, VOL. 104, NO. B7, PAGES 15,089–15,104, JULY 10, 1999

Constraints on the origin of slab and mantle wedge anomalies in Tonga from the ratio of S to P velocities

Keith D. Koper[1] and Douglas A. Wiens

Department of Earth and Planetary Sciences, Washington University, St. Louis, Missouri

LeRoy Dorman, John Hildebrand, and Spahr Webb

Scripps Institution of Oceanography, La Jolla, California

Abstract. We examine two prominent upper mantle velocity anomalies in the southwest Pacific, the Tonga slab anomaly and the corresponding overlying mantle wedge anomaly, using data collected during a combined land-sea deployment of temporary seismometers. The linear geometry and small interstation spacing of the instruments yield high-resolution data along a cross section of the Tonga subduction zone, including the actively spreading Lau back arc basin. We estimate the relative variation of P and S velocity, often described as $\nu = \delta \ln V_s / \delta \ln V_p$, for the slab and mantle wedge anomalies using two distinct methods: a linear regression of the P and S travel time residuals, and detailed modeling of the velocity structure using a three-dimensional finite difference travel time algorithm. The two methods yield similar results, with ν of the slab being 1.1-1.5 and ν of the mantle wedge being 1.2-1.3. These values are consistent with experimental data concerning the effect of temperature on P and S wave velocities in the upper mantle and are lower than what is expected for velocity anomalies generated by the presence of partial melt. These observations imply that either the theoretical estimates of ν for partial melt are too large or very little partial melt is present beneath the Lau basin. In the latter case, melt must be quickly removed from the rock matrix, such that the velocity anomalies are due to increased temperature, and not melt. The bulk of the velocity anomaly in the mantle wedge can be explained by temperature anomalies of 400-600°C because of the amplification of temperature derivatives of seismic velocity by anelastic effects. Such large thermal anomalies, generated by decreased lithospheric thickness and mantle upwelling beneath the fast spreading Lau back arc basin, can still leave the mantle near the solidus, even after accounting for the effect of increased volatile content in the mantle wedge. The lower-amplitude velocity reductions in the deeper wedge are likely related to an increased concentration of volatiles from the subducting slab.

1. Introduction

The modeling and interpretation of seismic travel times is ubiquitous in body wave studies of Earth structure. Of particular interest is the relative variation of P and S wave travel times, since by combining both types of data it may be possible to place constraints on the cause of a particular velocity anomaly, rather than simply estimating its magnitude. For example, *Hales and Doyle* [1967] analyzed the relative variation of teleseismic P and S wave travel time residuals to suggest that partial melt is present beneath the western United States; *Suyehiro and Sacks* [1979] modeled P and S travel times from deep events in the Japan subduction zone and inferred that temperature alone cannot account for the velocity contrast between the subducting slab and overlying mantle wedge; *Zhao et al.* [1996] combined P and S wave tomography to resolve a large Poisson's ratio anomaly near the epicenter of the Kobe earthquake, perhaps due to the presence of fluids; *Su and Dziewonski* [1997] inverted for global mantle models of shear and bulk velocity to investigate the nature of long-wavelength velocity anomalies in the lower mantle.

The purpose of this work is to exami15089 relative variation of two prominent upper mantle velocity anomalies in the southwest Pacific, the Tonga slab and

[1] Now at Department of Geosciences, University of Arizona, Tucson

Paper number 1999JB900130.
0148-0227/99/1999JB900130$09.00

overlying mantle wedge anomalies, using a set of high-quality P and S wave travel times. The arrival times are hand-picked from the waveforms of a series of deep and intermediate-depth events which occurred in the subducting Tonga slab during two temporary deployments of seismometers in late 1994. The small interstation spacing (~40 km) and linear geometry of the arrays (Figure 1) generates high-resolution data across a two-dimensional slice of the Tonga subduction zone.

The Tonga mantle wedge and slab anomalies are opposite in sign and may have fundamentally different causes. Conventional wisdom attributes the slab anomaly to the relatively cool temperature of subducting lithosphere, and previous work with this data set [*Koper et al.*, 1998] has indicated that the P wave travel time data is well fit by velocity models constructed with simple thermal and petrological constraints. It is also possible, though, that mineralogical differences between the slab and ambient mantle, or isochemical, isobaric phases changes [*Anderson*, 1987] play a significant role in generating slab velocity anomalies. By analyzing the relative variation of P and S travel time residuals and using laboratory data on the elastic behavior of rocks and mantle minerals [e.g., *Kern and Richter*, 1981; *Anderson et al.*, 1992], we can infer if direct temperature effects are a sufficient explanation of the slab anomaly. Likewise, we can examine the variation of residuals across the Lau back arc basin, the location of fast back arc spreading [*Bevis et al.*, 1995; *Taylor et al.*, 1996] to ascertain the nature of the mantle wedge anomaly. If the bulk of the mantle wedge anomaly results from partial melt, then the relationship between P and S residuals should be distinctly different from that predicted for a thermally induced velocity anomaly.

We analyze the Tonga travel time data using two approaches. The first is a straightforward comparison of the relative magnitude of the S and P residuals similar to the method used by *Hales and Doyle* [1967]. We use an iterative gradient search, taking into account uncertainties in both variables, to define the S residual as a linear function of the P residual. The slope of this line, which is insensitive to uncertainties in the hypocentral parameters of the Tonga earthquakes, is a direct estimate of the ratio of velocity anomalies. This method requires no a priori constraints on the velocity structure of the Tonga subduction zone, though it does require similarity between the ray paths of P and S waves. The second approach is an extension of previous modeling of the Tonga data [*Koper et al.*, 1998]. We independently model the P and S travel time residuals using a 3-D finite difference algorithm [*Vidale*, 1990; *Hole and Zelt*, 1995] to compute synthetic travel times for various velocity models. We use thermal, mineralogical, and morphological constraints to construct the P and S velocity models, and we do a grid search to find optimal values of the model parameters that control the magnitude of

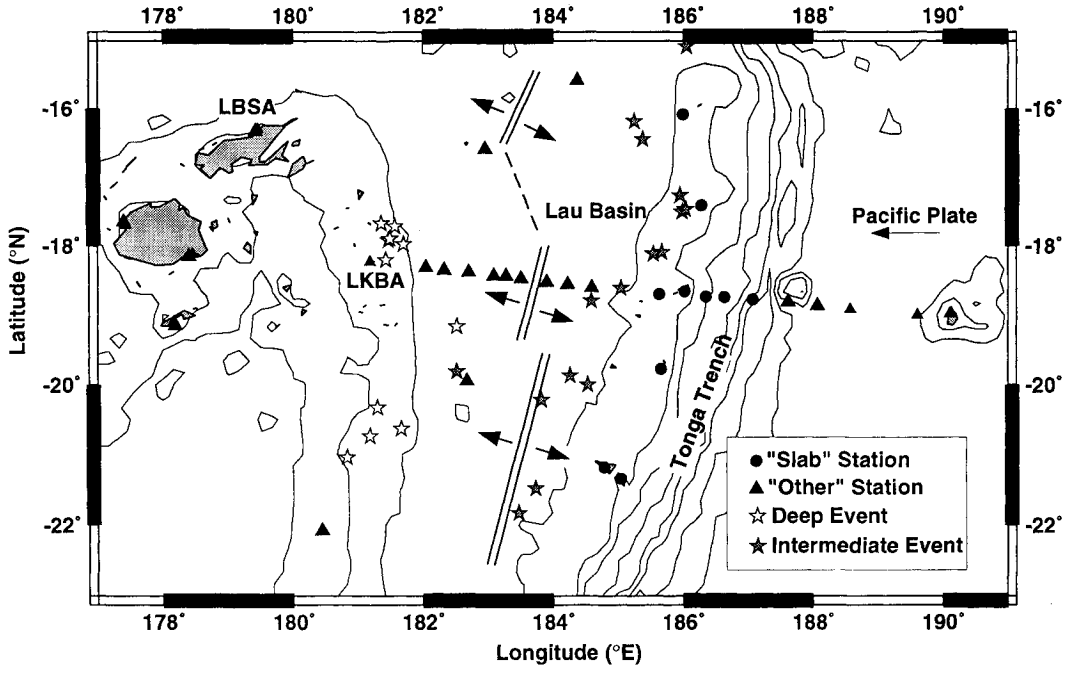

Figure 1. Station geometry of the Southwest Pacific Seismic Experiment (SPASE) and Lau Basin Ocean Bottom Seismometer deployments. The bathymetry of the region is shown with contour intervals of 1500 m. Travel times from the deep events that are recorded at the "slab" stations are indicative of ray paths which are almost entirely contained in the slab. Ray paths from the intermediate events to the Fiji stations LKBA and LBSA are almost entirely contained in the low-velocity mantle wedge region. The ray paths from deep events to the back arc stations sample a combination of deep slab and mantle wedge structure but are more sensitive to the velocities in the mantle wedge below the spreading center.

the slab and mantle wedge velocity anomalies. Unlike the first analysis, this method depends on a priori information about the Tonga velocity anomalies; however, it does not require assumptions about the ray paths of the P and S waves.

Both methods have advantages over directly comparing P and S wave tomographic images. Seismic tomography resolves the spatial structure of velocity heterogeneity better than the magnitude of heterogeneity. Tomographic estimates of the magnitude of velocity anomalies may be biased by the particulars of the inversion such as damping parameters and the choice of starting model, and even if identical techniques are used for P and S waves, differences between the P and S data sets will render anomaly amplitudes differently in the two models. Furthermore, it is not feasible to perform S wave travel time tomography with the Tonga data set because only the largest earthquakes produce good S wave arrivals at stations in the low-Q back arc basin and so leave a very sparse S wave data set. Therefore we use a small, high-quality collection of P and S wave travel times to compare the relative velocity variations.

2. Data

Data used in this study were recorded during the Southwest Pacific Seismic Experiment (SPASE) [*Wiens et al.*, 1995] and Lau Basin Ocean Bottom Seismometer (OBS) deployments in 1993-1995. The SPASE project consisted of a 2-year deployment of 11 broadband seismographs, and the Lau OBS project consisted of 30 three-component 1-Hz seismographs deployed for 3 months. The station geometries of the deployments are illustrated in Figure 1, along with the epicenters of the 27 deep and intermediate depth events used in this study (Table 1). Only events that generated a significant number of teleseismic arrivals are chosen, since such data are crucial for generating high-quality locations.

We use three different groupings of the data for the three main analyses. For the residual slope analysis of the slab velocity anomaly, we use 78 P and S wave arrival times from 11 deep events that occurred during the 3-month period of overlap between the SPASE and Lau basin OBS deployments. The arrival times are picked from stations near the Tonga Trench (Figure 1); thus these rays travel almost entirely within the high-velocity Tonga slab. For the residual slope analysis of the mantle wedge anomaly we use arrival times recorded at Fiji land stations LKBA and LBSA from 16 large intermediate events which occurred during the 2-year SPASE deployment, yielding 23 P and S wave arrival times. The ray paths from these events are almost entirely within the low-velocity mantle wedge region, beneath the active Lau back arc spreading center.

Table 1. Events Studied

Origin				
Day	Time, UT	Latitude, °S	Longitude, °W	Depth, km
94/005	08 14:45.9 (2)	18.61	174.96	260
94/019	01 18:57.1 (2)	20.00	175.47	223
94/055	15 25:36.7 (2)	17.50	174.01	129
94/056	00 40:30.6 (2)	17.47	173.96	125
94/071	09 39:29.4 (2)	20.22	176.18	280
94/223	19 32:53.4 (2)	21.83	176.53	182
94/236	03 46:21.9 (2)	16.18	174.75	305
94/272	17 16:06.5 (1,3)	17.80	178.52	563
94/273	19 30:18.5 (1,3)	21.08	179.12	626
94/274	14 54:29.6 (1,3)	18.20	178.39	642
94/289	12 40:42.8 (1)	17.91	178.53	563
94/292	06 06:24.8 (1)	19.34	177.41	569
94/313	14 41:44.1 (1,3)	17.84	178.38	600
94/319	14 37:07.1 (1,3)	20.85	178.74	603
94/326	05 04:21.7 (1,3)	20.64	178.31	538
94/331	11 39:55.1 (1)	20.51	178.50	602
94/334	06 37:18.9 (1,3)	17.99	178.26	606
94/336	12 54:52.1 (1)	17.98	178.29	595
94/355	20 34:16.9 (2)	19.87	175.74	247
95/075	04 34:46.2 (2)	21.48	176.27	184
95/137	03 52:56.8 (2)	15.08	173.95	123
95/145	03 14:54.9 (2)	18.79	175.41	242
95/174	10 15:18.0 (2)	18.09	174.33	128
95/196	01 35:16.5 (2)	19.81	177.48	369
95/197	23 46:55.6 (2)	18.11	174.46	131
95/207	09 09:51.8 (2)	16.44	174.62	239
95/216	10 31:23.9 (2)	17.26	174.05	138

15091

Day is year and day of year. Numbers in parentheses refer to the group that the data belong to.

For the finite difference travel time analysis of the entire region we use 146 P wave and 129 S wave arrival times recorded across the linear array of seismometers from the seven best located, deep events. Because this procedure is more dependent on event location than the residual slope analysis, we use a smaller, better located group of earthquakes. The ray paths from these events sample a combination of slab and mantle wedge structure.

For each P and S arrival time we define an uncertainty between 0.1 s and 1.0 s based on the quality of the pick. We use these uncertainties as weights in generating the linear relationship between P and S residuals, as well as in relocating the events. There are several reasons why the P wave arrival times are more accurate than the S wave arrival times: (1) the S waves are more attenuated and emergent than the P waves, especially at stations in the back arc basin, (2) often a significant P wave coda exists when the S wave arrives, (3) the S arrivals are picked from horizontal components, which have a larger background noise level, and (4) S waves are subject to the effects of transverse anisotropy. *Fischer and Wiens* [1996] and *Smith et al.* [1998] report shear wave splitting times of 0.5-1.8 s for intermediate and deep Tonga events recorded at the Fiji stations and OBSs; however, for the ray paths used in this study the vast majority of S wave arrival times differ by <1 s between horizontal components. In cases where the arrival times are different, we choose the earlier of the two. Since the raw S wave anomalies range up to 10 s, the uncertainties posed by splitting are small relative to the velocity heterogeneity signal.

3. Slope Analysis of Travel Time Residuals

By Fermat's principle the path a seismic ray travels represents a stationary point with respect to travel time; thus the derivative of travel time with respect to path geometry is small near ray paths. Because of this, changes in ray paths induced by velocity heterogeneities give rise to second-order effects in travel time residuals. To first order the perturbation in travel time (δt) for a given perturbation in velocity (δv) is given by

$$\delta t = -D\frac{\delta v}{v^2}, \tag{1}$$

where v is the path-averaged velocity in a reference model and D is the path length of the seismic ray. Assuming that the effect of different path geometries is much smaller than the effect of anomalous velocities, a linear relation exists between the P and S residuals, $\delta t_s = a\delta t_p + b$, with a an explicit function of the relative variation of velocities [*Hales and Doyle,* 1967],

$$a = \frac{\delta V_s}{\delta V_p}\frac{V_p^2}{V_s^2}. \tag{2}$$

The ratio V_p/V_s varies only slightly in the upper mantle; for example, V_p/V_s ranges from 1.73 to 1.85 in the upper mantle of the IASP91 model [*Kennett and Engdahl,* 1991]. Because of this, observed values of a are primarily indicative of the relative size of the P and S velocity anomalies and thus sensitive to their underlying cause. Note that $a = \nu(V_p/V_s)$, where ν is a parameter that is often used in interpreting global tomographic models and is defined as $\delta \ln V_s/\delta \ln V_p$. Throughout this paper we compare a and ν values assuming V_p/V_s is 1.75. Using a slightly different value of V_p/V_s does not significantly change the results.

Interpretation of the intercept b is more difficult. If the residuals are calculated with respect to a velocity model that is a poor average representation of the region, then it is possible that nonzero values of b are produced; however, these values are not necessarily indicative of velocity heterogeneities but are rather due to inadequacies in the reference model [*Hales and Doyle,* 1967]. *Romanowicz and Cara* [1980] find that for sufficiently complex lateral velocity variations, b is theoretically nonzero, and its value can be directly related to velocity perturbations. In this work, however, we interpret only the first-order velocity heterogeneities defined by a and do not use b values for quantitative analysis of the velocity anomalies.

Previous work on the relative variation of P and S travel time residuals (or station corrections) has generally been carried out on a larger scale than in the work presented here. Several researchers have estimated a on a continental scale, using either hand-picked arrival times or carefully selected International Seismological Centre (ISC) times, reporting values of ~3.5-4.5 for Canada, the United States, and Europe [*Doyle and Hales,* 1967; *Hales and Roberts,* 1970; *Jeffreys and Singh,* 1973; *Romanowicz and Cara,* 1980; *Wickens and Buchbinder,* 1980; *Souriau and Woodhouse,* 1985]. A global estimate of a, 3.61 ± 0.13 [*Souriau and Woodhouse,* 1985], derived using P station corrections and a tomographic mantle S wave model [*Woodhouse and Dziewonski,* 1984], is also in this range. These a values correspond to ν = 1.9-2.5, a result which is seemingly confirmed by long-wavelength, global mantle models, which report ν values of 2.0-2.5 [*Dziewonski and Woodhouse,* 1987; *Giardini et al.,* 1987; *Li et al.,* 1991]. However, the ν values from the low-order mantle models are more indicative of lower mantle variations, while the ν values from the residual slope analyses are more indicative of upper mantle variations, so it is not clear that they should be expected to agree. *Robertson and Woodhouse* [1996] have recently performed a joint inversion of P and S arrival times for 3-D mantle velocity models and find that ν linearly increases from 1.7 to 2.6 in the depth range of 700 to 2600 km, implying that ν is smaller in the upper mantle than in lower mantle, as is expected for thermally induced velocity anomalies [e.g., *Agnon and Bukowinski,* 1990; *Isaak et al.,* 1992]. This is further supported by the forward modeling work of *Bokelmann and Silver* [1993] who find $\nu \sim 1.7$ for a

specific region (the Caribbean) in the uppermost lower mantle. However, in contrast to *Roberston and Woodhouse* [1996], *Kennett, et al.* [1998] jointly inverted P and S wave travel times from the ISC with a high-resolution cellular parametrization and found no depth dependence for depth-averaged values of ν (a nearly constant average of 2.1) but did report large lateral variations in a given layer.

The likely explanation for large values of a reported by previous researchers is the broadness of the regions from which data were used. If ν, and thus a, has significant variation on a scale that is smaller than the model region, then the observed values may not be useful for making inferences on the underlying causes of velocity anomalies. For instance, *Romanowicz and Cara* [1980] report $a = 4.75 \pm 1.0$ for North America as a whole, but when the data are separated into geographical regions, they find values of 2.54 ± 0.8 ($\nu \sim 1.5$) for the western province and 2.33 ± 1.1 ($\nu \sim 1.3$) for the central eastern province. This is important in the sense that the overall value (4.75) is vastly different from the average of the two provinces (2.44) and probably is not indicative of any velocity heterogeneities but is simply an artifact of combining disparate tectonic regions. Similarly, *Souriau and Woodhouse* [1985] report a large variation in a values (2.44-5.69) when the data are binned according to various, well-sampled, tectonic provinces (i.e. subduction zones, shields, oceans). Most recently, *Robertson and Woodhouse* [1997] find a global value of $a = 2.85$ ($\nu \sim 1.6$), significantly lower than previous global estimates and close to the regional estimates of *Romanowicz and Cara* [1980], when tectonic regionalization of the data is accounted for and high-quality data are used.

3.1. Estimating ν for the Tonga Slab

We examine the Tonga slab anomaly by analyzing P and S residuals only from stations that record phases which have primarily sampled the slab (group 1 of the data in Table 1). Waveforms recorded at these near-trench stations have higher frequency contents and more negative travel time residuals than those recorded at neighboring stations, indicating that they are representative of the slab anomaly. By using events and stations which vary in distance along strike, a wide range of P and S residuals is observed, making the relationship between the two (Figure 2) robust. We fit a line to these data by minimizing the sum of the weighted, squared errors (equation (7) of *York* [1966]) using a modified gradient search algorithm which accounts for the designated uncertainties in both the P and S residuals. The best fitting values for a and b are reported in Table 2, along with standard error estimates generated using a bootstrap (data resampling with replacement) technique. These standard errors are only indicative of uncertainties in the arrival time picks themselves and do not account for uncertainties in the residuals caused by mislocation related to velocity heterogeneities in the Earth.

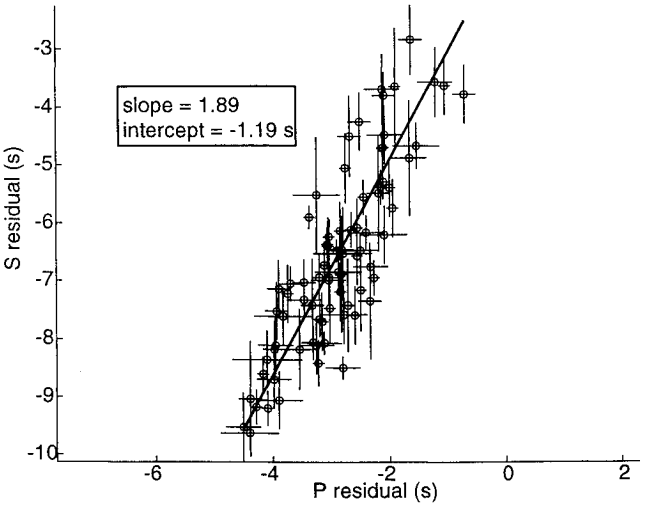

Figure 2. P and S travel time residuals from the group 1 events. A total of 78 P and S wave travel times, generated from 11 deep events and recorded at the 10 "slab" stations are shown. The error bars are defined by uncertainties in the arrival time picks. These residuals are defined based on the least biased locations: only teleseismic P waves and and P waves recorded at the Fiji stations were used. A gradient search algorithm which accounts for uncertainties in both types of residuals was used for the linear regression. The slope of this line, which is insensitive to uncertainties in the hypocentral parameters, provides an estimate of ν for the slab.

To investigate the effect of systematic mislocation on the values of a and b, we relocate the events in three different ways using the IASP91 velocity model. In the first relocation we include only teleseismic data and the P waves recorded at the Fiji stations. The Fiji stations are the least biased of the local stations, since they are located near neither the slab nor the back arc spreading center, and provide a strong constraint on the depth of the events in the location process. Next, we add the remaining local P waves to the set of arrival times and relocate the events. Many of these times are biased by the slab anomaly and cause the locations to move to the east and upward [*Koper et al.*, 1998]. The third set of locations is constructed by including all the local S wave arrival times as well the P wave data. This further biases the locations because the slab anomaly has a larger effect on S wave residuals than on P wave residuals. The best fitting values for a and b, as well as the mean P and S residual of the slab stations, are presented in Table 2 for each of the three cases. The primary effect of systematic bias in the locations of the events is to change the magnitude of the travel time residuals but not their relative variation. The absolute values of the slab residuals are greatly reduced when biased arrival times are included in the relocations; however, the value of a varies only from 1.86 to 1.97. Thus the fact that we approximate the velocity structure of

Table 2. Results of Travel Time Residual Analysis

Set of Residuals	Data Used in Relocation	Slope a	Intercept(s) b	Mean of P Residuals, s	Mean of S Residuals, s
Slab	teleseismic and Fiji stations P waves	1.89 ± 0.09	-1.19 ± 0.28	-2.9	-6.6
Slab	all P waves	1.97 ± 0.12	-1.61 ± 0.20	-1.5	-4.5
Slab	all S and P waves	1.86 ± 0.11	-1.78 ± 0.14	-0.5	-2.8
Mantle Wedge	all P waves	2.00 ± 0.19	0.08 ± 0.52	2.3	4.8
Mantle Wedge	all S and P waves	2.14 ± 0.25	0.01 ± 0.47	1.3	2.9

the Tonga subduction zone with a 1-D reference model (IASP91) for the purposes of event location does not influence the relative variation of velocities as measured by a.

We next examine the effect of random uncertainties in hypocentral parameters on the relative variation of P and S residuals using a stochastic procedure. For each group 1 event we randomly vary the hypocentral parameters within ranges that are typical of the standard location errors for these events (determined from uncertainties in arrival time data): latitude and longitude $\pm$ 0.2°, depth $\pm$ 5 km, and origin time $\pm$ 0.25 s. We implement this procedure 10 times for each of the location types described above and compute the corresponding values of a and b. The maximum change in a for the 10 samples is only 0.2-0.25 for the three location types, comparable to the standard errors defined for the linear fits.

Thus the relative variation of P and S travel time residuals produced by the slab velocity anomaly a is insensitive to hypocentral uncertainties and uncertainties in the arrival time picks themselves. Systematic location errors produce uncertainties of 0.1-0.2, random location errors produce uncertainties of 0.2-0.25, and the direct effect of arrival time uncertainties produce uncertainties of 0.1-0.15. The range of a values we observe for the Tonga slab (1.86-1.97) imply that ν_{slab} is 1.1-1.2.

The intercept estimates for the slab anomaly b vary from -1.19 s to -1.78 s for the three location types and have standard errors of 0.2-0.3 s. To investigate the significance of these values, we perform linear regressions with the intercept constrained to be zero. The a values we retrieve (2.3-3.2) are higher than in the two-parameter case, but the variance reduction is significantly worse, as quantified by an F test, than in the two-parameter case. Thus b for the slab is significantly different than 0 and may be a function of the slab velocity anomaly or source location errors.

3.2. Estimating ν for the Tonga Mantle Wedge

We analyze travel time residuals induced by the mantle wedge velocity anomaly using 22 residuals recorded at LKBA and LBSA (Figure 3) from intermediate-depth events (group 2 in Table 1). The ray paths have primarily sampled the upper 200 km of the mantle wedge, including the region directly beneath the Lau spreading center where velocities are the slowest [*Zhao*

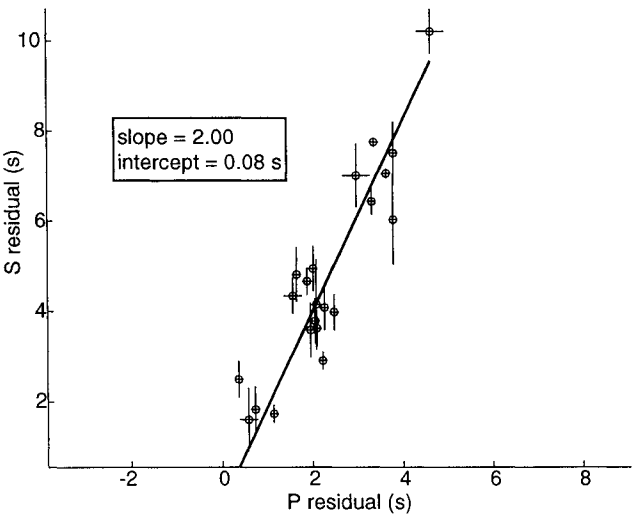

Figure 3. P and S travel time residuals from the group 3 events. These 23 P and S wave residuals were recorded at the Fiji stations LKBA and LBSA from 16 intermediate depth events. The error bars are defined by uncertainties in the arrival time picks. The positive residuals are indicative of the low-velocity mantle wedge region. A wide range of values is obtained by using an array of sources which varies substantially along strike. These residuals are based on locations defined using both teleseismic and local P wave data. Including S wave arrival times in the locations [15094] does not significantly affect the the value of the slope derived from the linear regression.

et al., 1997; *Xu and Wiens*, 1997]. We include only the largest intermediate-depth events since the S waves from smaller events are difficult to pick accurately owing to high attenuation. We do not include residuals from deep events that are recorded by the back arc stations because these ray paths sample a combination of deep slab and mantle wedge structure and thus do not isolate the velocity anomaly as well as the ray paths from the intermediate-depth events.

It is difficult to achieve high-quality locations for the intermediate events using only teleseismic and Fiji station arrivals, as we did for the deep events (group 1 data), so we initially relocate the events using all available P wave data, including teleseismic pP observations. Next, we relocate the events using all available S wave arrival times as well as the P wave data. This creates more bias in the data because of the larger magnitude of the mantle wedge-induced (mw) S residuals; however, both location types yield similar values for a_{mw} (Table 2). This indicates that the main effect of using a reference Earth model to define the travel time residuals biases their absolute magnitudes and not their relative variation, the same result that was obtained with the slab-induced residuals. We apply the stochastic procedure described in section 3.1 and find small errors associated with random hypocentral uncertainty, with a changing by $\sim \pm 0.25$. Thus the value of a_{mw} is stable with respect to systematic location bias and random location errors. The two values we observe for a_{mw}, 2.00 and 2.14, imply that ν_{mw} is in the range of 1.2 to 1.3, only slightly higher than our estimates of ν_{slab}.

In contrast to the results for the slab data the b values for the mantle wedge regressions are nearly zero, with values of 0.01 and 0.10 for the two location types. The standard errors for these values, 0.5 in both cases, indicate that b is not significantly different than zero. To further check this, we perform a regression with b constrained to be zero. We achieve only slightly different a values than in the two-parameter case, 2.15 and 2.03, and an F test indicates that the variance reduction in using two parameters is not significant at the 95% level. Thus the mantle wedge anomaly produces a direct correlation between P and S residuals with no baseline difference.

3.3. Estimating a Combined Regional ν

Since our estimates of ν_{slab} and ν_{mw} are similar, it is possible that the velocity heterogeneities in both regions have the same cause and the two regions can be combined in a single analysis. To compute an overall ν, we use the same set of 11 deep earthquakes that we used in estimating ν_{slab}; however, we now include travel time residuals recorded by all of the SPASE land stations and OBSs (Figure 1). This produces a total of 203 P and S wave travel times. The ray paths sample the slab, a combination of slab and mantle wedge structure, and the relatively homogeneous upper mantle beneath Fiji. The relative residuals, shown in Figure 4, have a slope of 2.39 ± 0.06, corresponding to $\nu \sim 1.4$, with a b value not significantly different than zero. As was the case with ν_{slab} and ν_{mw}, this value does not significantly change if different data sets are used in the relocations: the slope increases to 2.56 if locations are generated by using local S arrivals as well as P arrivals. The similarity of this ν value to ν_{slab} and ν_{mw} is consistent with the same mechanism being responsible for both the Tonga slab anomaly and the overlying mantle wedge anomaly.

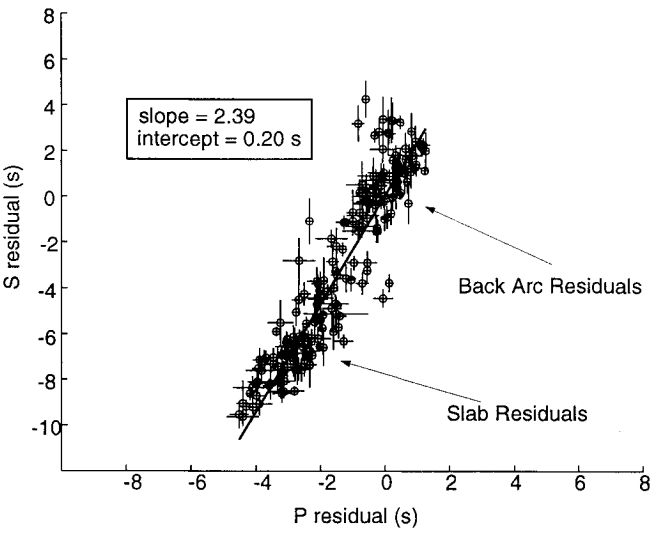

Figure 4. P and S travel time residuals from the 11 deep events recorded at all of the stations. Simultaneously fitting a line to these two populations of residuals gives a slope that is nearly equal to the slopes estimated for each region individually. This is consistent with the two regions, slab and back arc/mantle wedge, having similar types of velocity anomalies.

4. Three Dimensional Modeling of Velocity Structure

The second analysis of the Tonga data consists of detailed modeling of the P and S wave velocity structures using 3-D finite difference code to compute first arriving travel times. This method requires a priori information on the structure of the Tonga subduction zone, but it is not subject to the assumption of similar path geometries for the P and S waves. We assume that the slab anomaly is due to a thermal anomaly, with variable magnitude, and that the mantle wedge anomaly has the depth dependence derived from waveform inversion by *Xu and Wiens* [1997] with variable amplitude. We perform a series of independent grid searches using P and S wave travel time data from the largest (best located) deep earthquakes in the Tonga data set (group 3 in Table 1). We estimate ν_{slab} and ν_{mw} by comparing the optimal values of the model parameters that control the slab and mantle wedge velocity anomalies.

We define the travel time residuals using the least biased of the locations discussed earlier, i.e., those in which only teleseismic data and P waves recorded at

the Fiji stations are used in the location. Since accurate locations cannot be determined for some of the smaller events without including the biased local arrival times, we have reduced the data set to travel times from only the larger, better located events, yielding a total of 146 P and 129 S residuals (Figure 5). This leads to a data set that is slightly different from that in our previous work [*Koper et al.*, 1998] in which the biased locations of the smaller events were accounted for by applying a relocation operator to the synthetic residuals.

4.1. Construction of Velocity Models of the Tonga Subduction Zone

A complete description of the construction of velocity models of the Tonga subduction zone is given by *Koper et al.* [1998], and so we only briefly discuss the constraints here. The morphology of the slab is determined from a database of local seismicity (J. J. McGuire, unpublished data, 1995), the thermal structure is determined with code developed by N. H. Sleep and K. C. Creager based on the finite difference algorithm of *Toksöz et al.* [1973] and using a plate model [*Stein and Stein*, 1992] for the initial lithospheric profile, and the mantle wedge low-velocity zone is modeled after the work of *Xu and Wiens* [1997]. Since topography on the 410-km discontinuity does not produce a discernible signal in the arrival time data [*Koper et al.*, 1998], we fix the discontinuity at an equilibrium position (uplifted) assuming a Clapeyron slope of 3.0 MPa/K, and the preliminary reference Earth model (PREM) [*Dziewonski and Anderson*, 1981] pressure model. Equilibrium models are implicitly faster than metastable wedge velocity models or models with no 410-km discontinuity topography; thus the best fitting temperature derivatives are biased toward smaller magnitude values. Given a specific velocity model, we calculate first arriving P and S wave travel times using a 3-D finite difference approach [*Vidale*, 1990; *Hole and Zelt*, 1995].

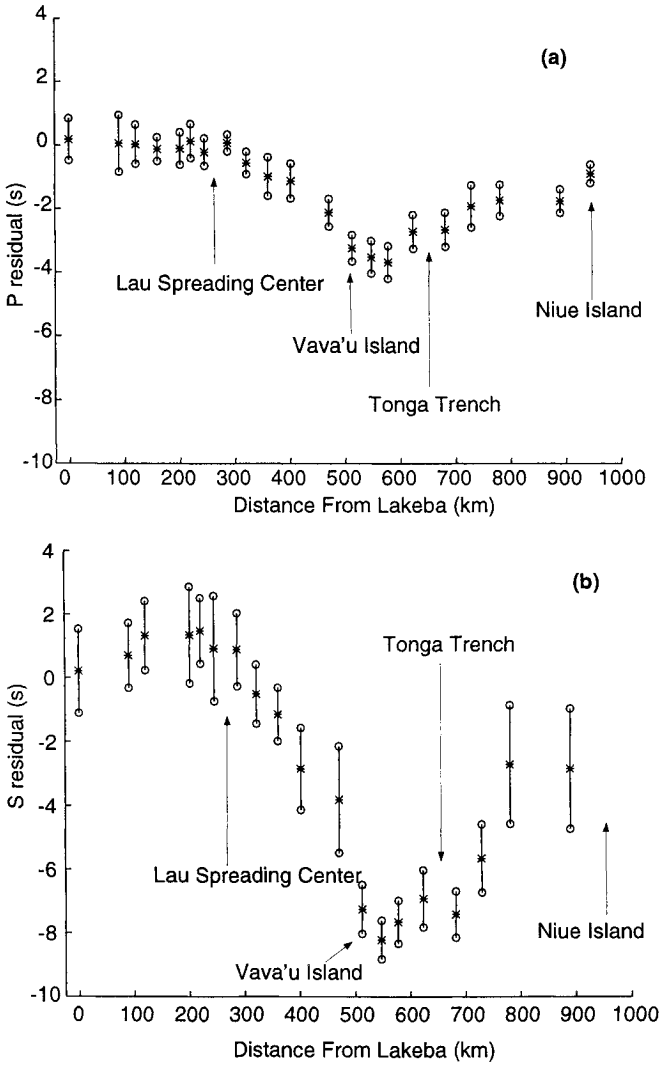

Figure 5. Mean travel time residuals from the group 2 events, averaged across the seismometer line, for (a) P waves and (b) S waves. Error bars represent ± 1 s.d. of the observed residuals at each station. The residuals are defined using the least biased locations, as discussed in the text. The slab anomaly is clearly indicated by the pronounced drop in residuals near the Tonga Trench.

Each velocity model evaluated in the grid search is completely determined by the values of three parameters (dV/dT, A_{lvz}, and a shift value) related to the above mentioned a priori constraints. The effect of temperature on the slab velocity structure is determined by assuming a value for dV/dT (either S or P). The S/P ratio of thermal derivatives, multiplied by V_p/V_s, gives an estimate of ν_{slab}. Although the best fitting values of the thermal derivatives found from the grid search depend on the thermal, mineralogical, and morphological constraints, the ratio of the two, and thus ν, is much less model dependent. We define the mantle wedge velocity model by choosing a value for A_{lvz} (either S or P), which is a number between 0 and 1 representing the amplitude of the anomaly in the low-velocity zone (lvz). A value of 1 corresponds to the exact model of *Xu and Wiens* [1997], while a value of 0.5 implements an anomaly half as strong in amplitude but with the same depth distribution. Setting A_{lvz} equal to zero gives a model with regular IASP91 velocities in the backarc. The ratio of the S wave value of A_{lvz} to the P wave value of A_{lvz} gives ν_{mw}. We allow the S wave model to vary from that of *Xu and Wiens* [1997] because of strong anisotropy in the Lau Basin. A model for the SH velocity from waves that generally travel horizontally through the Lau basin (Y. Xu, unpublished work, 1997) is significantly faster than the SV model reported by *Xu and Wiens* [1997]. Since our data travel vertically and are polarized nearly horizontally, we expect faster S wave velocities and thus a smaller velocity anomaly than observed by *Xu and Wiens* [1997]. The third parameter, the shift value, allows the entire slab structure to translate perpendicular to strike, accounting for uncertainties in the morphological model as well as uncertainties in the positions of the epicenters relative to the velocity anomalies [*Koper et al.*, 1998].

4.2. Results of Grid Searches for P and S Wave Velocity Models

We perform independent grid searches to find the best fitting model parameters for the P and S wave data. We vary the parameters in the same manner for both types of data: A_{lvz} is varied from 0.2 to 1.0 with increments of 0.2, dV/dT is varied from -0.5 to -0.1 $\mathrm{ms^{-1}K^{-1}}$ in increments of 0.1 $\mathrm{ms^{-1}K^{-1}}$, and three shift values representing a range of 40 km are used. A cross section of the error landscape of the two searches is shown in Figure 6.

We perform two additional grid searches, on both data sets, with progressively smaller increments in the model parameters, giving about 350 model evaluations. We center the search intervals for the model parameters on the best fitting values from the previous grid search. The best P model reduces the root-mean-square error of the residuals from 2.02 s to 0.57 s (72%), while the best S wave model reduces the error from 4.86 s to 1.32 s (73%). These models are illustrated in Figure 7. The remaining travel time residuals are probably due to shallow site effects that were not accounted for in our modeling, as well as uncertainties in the arrival time picks.

To estimate the effect of arrival time uncertainty on the optimal parameter values, we use a stochastic, resampling method based on the bootstrap technique. We construct an artificial data set of P and S travel times by generating a set of Gaussian random numbers using the actual travel time values as means and the designated uncertainties as standard deviations. We then compute the fit of each parameter combination with respect to the synthetic data and choose the one with the lowest value as the best solution. The procedure is repeated N times, and the mean and standard deviation of the model parameters of the population of best solutions are calculated. We use these standard deviations as proxies for the actual uncertainties in our model parameters. This procedure is computationally quick to implement because we do not have to recalculate the synthetic travel times for each parameter combination. We use $N = 500$ and find that the standard deviations of the model parameters converge after $\sim$ 200 iterations. Our model parameter estimates become $dV/dT = -0.23 \pm 0.01$ $\mathrm{ms^{-1}K^{-1}}$, $A_{\mathrm{lvz}} = 0.50 \pm 0.03$ for P waves, and $dV/dT = -0.20 \pm 0.01$ $\mathrm{ms^{-1}K^{-1}}$, $A_{\mathrm{lvz}} = 0.67 \pm 0.03$ for S waves.

These error estimates do not include the effect of uncertainties in our a priori constraints but only account for errors in the picking of arrival times and so are only lower bounds on the overall uncertainties. For example, by using a velocity model containing a metastable wedge of olivine, instead of the equilibrium-type models used in this study, optimal estimates of dV/dT for P waves can vary by as much as 0.175 $\mathrm{ms^{-1}K^{-1}}$ [*Koper et al.*, 1998]. Thus a range of -0.2 to -0.4 $\mathrm{ms^{-1}K^{-1}}$ is a more realistic estimate for the the possible values of

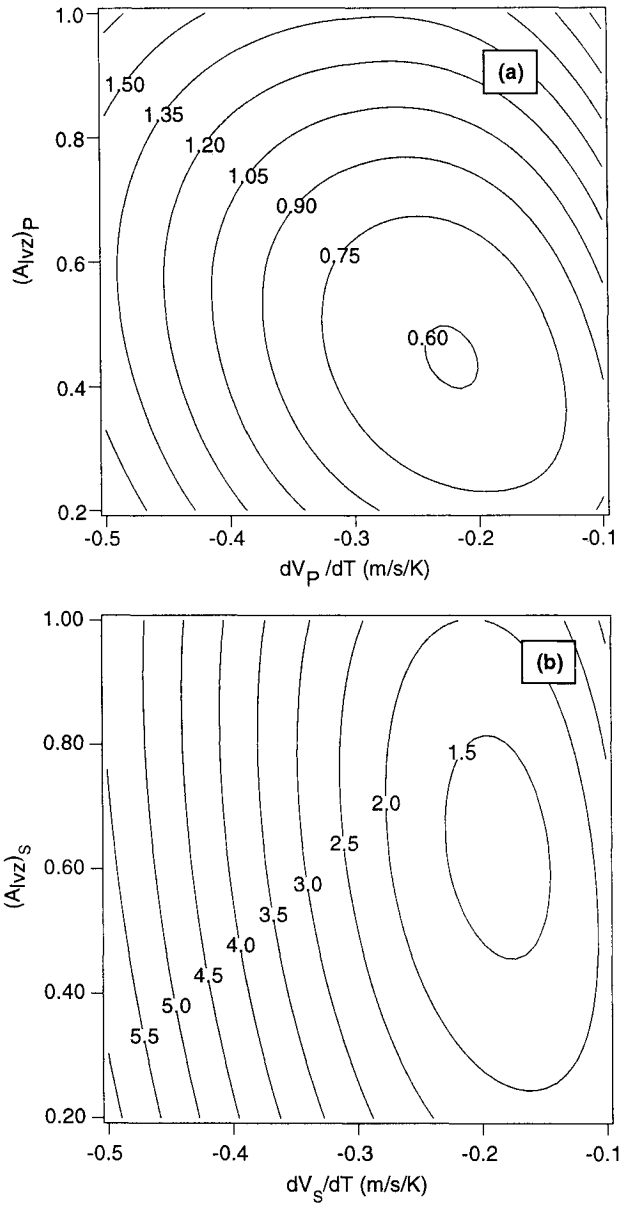

Figure 6. Results of the coarsest grid searches for (a) the P wave data and (b) the S wave data. The error landscapes are produced by averaging over the three shift values and then using bicubic interpolation to resample the 25 points to a much finer spacing. The contours represent error values defined as the root-mean-square difference of theoretical and observed travel time residuals. The trend of the contours indicates that $(A_{\mathrm{lvz}})_P$ and dV_P/dT are negatively correlated. This is opposite to the correlation of *Koper et al.* [1998] because no relocation operator was used in the present study.

of the temperature derivatives. The fact that we have used equilibrium type models, implicitly the fastest type of model because of the large uplift of the 410-km discontinuity, biases our temperature derivatives toward smaller magnitude values, but the ratio of derivatives, which determines ν_{slab}, is much less dependent on model assumptions.

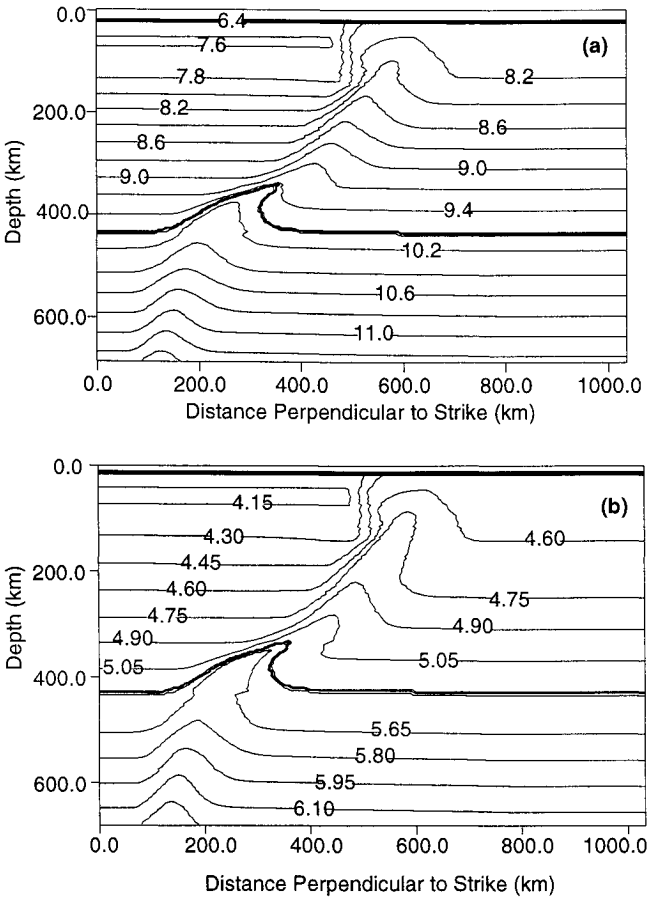

Figure 7. Cross sections of the optimal 3-D models found during the grid search for (a) P wave velocity and (b) S wave velocity. The velocities are shown having been flattened for use in a Cartesian grid. Travel time errors associated with applying an Earth flattening transformation to a 3-D velocity model are discussed by *Koper et al.* [1998]. Both models are equilibrium models meaning the 410-km discontinuity is uplifted because of the exothermic nature of the $\alpha \rightarrow \beta$ phase transition. Intraslab variations of the discontinuity are not resolvable with the Tonga travel time data set [*Koper et al.*, 1998]

The 1-D velocity models corresponding to the optimal A_{lvz} values are shown in Figure 8. The maximum velocity reduction is ~7% for P waves and ~10% for S waves. Our inferred S wave model is thus only ~70% as strong as the SV model of *Xu and Wiens* [1997]. Our model is comparable in magnitude to an SH model for the region constructed from waveform inversion (Y. Xu, unpublished work, 1997). Computing the S:P ratio of the amplitudes of the low-velocity zones gives ν_{mw} ~1.3, in good agreement with the residual slope analysis estimate of 1.2-1.3.

With the optimal temperature derivative values the maximum velocity increase in the slab is 3.3% for P waves and 5.1% for S waves. Thus the maximum velocity difference between the slab and the mantle wedge is ~10% for P waves and 15% for S waves. Using the S:P ratio of thermal derivatives yields $\nu_{\mathrm{slab}} \sim 1.5$, which is somewhat higher than our slope analysis estimate of ~ 1.1-1.2. The optimal parameter values for the P wave models are slightly different than those reported in our previous analysis [*Koper et al.*, 1998]. In that study we found $dV_p/dT = -0.27$ ms^{-1}K^{-1} for equilibrium models and a value of 0.40 for A_{lvz} which corresponded to a maximum P wave velocity decrease of ~5% in the mantle wedge. The discrepancy results from the use of slightly different sets of earthquakes and methodologies, but the differences are smaller than the effect of our particular model assumptions and so not significant.

The best fitting dV_p/dT value (-0.23 ms^{-1}K^{-1}) is lower than previous seismological estimates of dV_p/dT which include -0.5 ± 0.1 ms^{-1}K^{-1} [*Creager and Jordan*, 1986] and -0.5 ± 0.2 ms^{-1}K^{-1} [*Fischer et al.*,, 1991]. Both estimates were made using standard thermal models and a residual sphere analysis of travel times. Since that technique relies on teleseismic data, it is possible that heterogeneities away from the source could be mapped into near source contributions, artificially enlarging the slab anomaly [*Zhou et al.*, 1990; *Schwartz et al.*, 1991] and thus the magnitude of dV_p/dT. The estimate of dV_p/dT = -0.9 ms^{-1}K^{-1} for the Aleutian slab [*Sleep*, 1973] may be artificially enlarged because *Sleep* [1973] considered a slab thermal model that only extended to a depth of ~200 km. The dV_p/dT value reported here is consistent with laboratory estimates on a variety of rock samples [*Kern and Richter*, 1981] but slightly smaller than single-crystal elastic measurements [*Anderson et al.*, 1992]. Likewise, our estimated value of dV_s/dT (-0.2 ms^{-1}K^{-1}) is more consistent with the rock data than the single-crystal experiments; however, it is significantly smaller in magnitude than the value

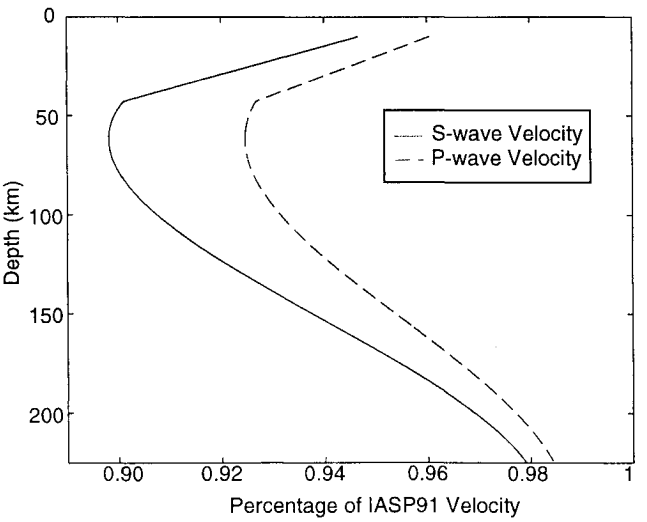

Figure 8. The optimal 1-D velocity models for the mantle wedge region. The models are scaled versions of the modeled derived by *Xu and Wiens* [1997] through waveform inversion. These models correspond to a constant ν value of ~1.2. The magnitude of velocity reduction trades off slightly with the magnitude of the slab velocity anomaly.

of -0.6 ± 0.1 $ms^{-1}K^{-1}$ reported by *McNutt and Judge* [1990] from a surface wave analysis of the Pacific ocean lithosphere.

5. Discussion

Both the residual slope analysis and the finite difference travel time modeling show that the relative variation of P and S velocities in the mantle wedge, as defined by ν, is in the range of 1.2-1.3. The ν estimates for the Tonga slab are less consistent, with the residual slope analysis yielding a value of 1.1-1.2 and the velocity modeling procedure yielding ~1.5. Nevertheless, a distinct change in ν between the slab and mantle wedge is ruled out. The type of velocity anomaly most consistent with ν = 1.1-1.5 is that due to a thermal perturbation.

5.1. Theoretical Estimates of ν for Thermal Anomalies

The theoretical ν value for thermally induced velocity anomalies is given by the S to P ratio of temperature derivatives of seismic velocity, scaled by V_p/V_s. Since V_p/V_s is relatively constant in the upper mantle, it is the ratio of thermal derivatives that controls the ν value. Excluding ab initio modeling, there are two main sources of information on the temperature derivatives of seismic velocity: (1) low-pressure, single-crystal elastic measurements of mantle minerals and (2) corresponding low-pressure measurements of igneous and metamorphic rocks. *Anderson et al.* [1992] summarize single-crystal elastic measurements on MgO, CaO, Al_2O_3, garnets, and two olivine samples and find that at low temperatures (300 K), dV_p/dT varies from -0.58 to -0.35 $ms^{-1}K^{-1}$, that dV_s/dT varies from -0.46 to -0.20 $ms^{-1}K^{-1}$, and that the S/P thermal derivative ratio is relatively constant varying from 0.55 to 0.95. At higher temperatures the magnitude of the derivatives generally decrease (except for the olivine derivatives), but the ratios are similar to the low-temperature case and vary from 0.55 to 0.84, except for Al_2O_3. This corresponds to a ν_{thermal} in the range of 0.95-1.6. For olivine, the dominant mineral in the upper mantle, a direct value of 1.18 is reported for ν_{thermal} [*Anderson et al.*, 1992].

Kern and Richter [1981] measured the low-pressure (6 kbar) elastic velocities of 15 igneous and metamorphic rocks, having a wide range of mineralogical and chemical composition, up to ~1000 K. The temperature derivatives of the seismic velocities are smaller than those derived from the single-crystal elastic data with dV_p/dT ranging from -0.40 to -0.17 $ms^{-1}K^{-1}$ and dV_s/dT varying between -0.39 and -0.15 $ms^{-1}K^{-1}$, but the S/P thermal derivative ratios of 0.59-0.89 are almost identical to the single-crystal data. (We do not consider three of the fifteen samples used by *Kern and Richter* [1981] that show anomalous values for the S/P thermal derivative ratio: two eclogite samples with ratios of 1.3 for which the measured dV_p/dT value is several times smaller than reported elsewhere [*Christensen*, 1979], and an amphibolite sample with a ratio of 1.9.) The most olivine-rich samples of *Kern and Richter* [1981] (dunite-1675 and peridotite-475) show a ν_{thermal} of 1.16 and 1.26, in close agreement with the single-crystal measurement of 1.18. Thus the laboratory estimates of the effect of temperature on the relative variation of velocities are in agreement and point to a general ν_{thermal} value of 0.9-1.6 and a value of 1.1-1.2 for olivine in particular.

There are two important considerations concerning the above mentioned experimental values. First, these values are measured at near zero pressure and so may not be valid at mantle pressures; however, although there is evidence that the magnitudes of temperature derivatives decrease with depth in the lower mantle [*Duffy and Ahrens*,1992, and references therein], it is likely that the pressure dependence of thermal derivatives in the upper mantle is small [*Knoche et al.*, 1997]. Second, the laboratory estimates of thermal derivatives of seismic velocity, and thus ν_{thermal}, are made at much higher frequencies than seismological observations and so do not include the anelastic effects of temperature anomalies [*Karato*, 1993]. At the lower seismic frequencies the dispersion associated with the increase of attenuation with temperature can significantly amplify the magnitude of the dV_p/dT and dV_s/dT, and so the effective thermal derivatives depend on Q, and ν_{thermal} depends on Q_p/Q_s [*Karato*, 1993]. Thus in the high-Q Tonga slab the laboratory values for ν_{thermal} should apply, while in the low-Q mantle wedge and back arc region, ν_{thermal} will be increased based on the relative attenuation of P and S waves. *Roth et al.* [1999] have inferred an average Q_p value of 150 and a Q_p/Q_s of 1.75 for the Tonga mantle wedge region. Using these numbers with *Karato's* [1993] calculations for olivine implies that ν_{thermal} should change from ~1.2 in the slab to ~1.4 in the mantle wedge, a difference that is comparable to the errors in our seismically determined values and so is not resolvable.

5.2. Theoretical Estimates of ν for Nonthermal Anomalies

Other possibilities for generating the large-scale velocity anomalies observed in Tonga include mineralogical variations and the presence of partial melt or fluid. Undulations in upper mantle discontinuities, including the Moho, or anisotropy induced by mantle flow in the region, cannot generate the observed amplitude and range of travel time residuals.

In the case of mineralogical variations it has previously been assumed that Poisson's ratio varies little between rock types, implying that V_p/V_s would be constant across velocity anomalies, yielding $\nu_{\text{chem}} \sim 1$ [*Hales and Doyle*, 1967; *Hales and Herrin*, 1972]. More recent work has shown that Poisson's ratio is quite dependent on chemical composition and t15099ere are significant crustal variations both on global scales [e.g., *Holbrook et al.*, 1992; *Zandt and Ammon*, 1995] and

regional scales [e.g., *Koch*, 1992]. These variations of Poisson's ratio are large enough that no general theoretical estimate of ν_{chem} can be made as is the case for ν_{thermal}. The variations are also large enough that distinct chemical heterogeneities can cause P and S wave residuals to become uncorrelated. That our data show a high degree of correlation (Figures 2, 3, and 4) implies that the Tonga velocity anomalies are not due to large changes in Poisson's ratio.

In the case of partial melt (pm), if the primary effect is on the shear modulus μ, then it is likely that ν_{pm}=1.5 to 2.25 [*Hales*, 1964]. A more sophisticated model of the effect of partial melt on seismic velocities gives $\nu_{pm} \sim 1.65$ [*Hales and Herrin*, 1972], and recent experimental work reports that melt tends to form in penny-shaped melt inclusions ($\nu_{\text{pm}} \sim 1.8$) rather than triple junction tubules ($\nu_{\text{pm}} \sim 2.3$) [*Faul et al.*, 1994]. (*Faul et al.* [1994] compute ν values for various melt geometries using the theoretical models of *Mavko* [1980].) These theoretical estimates for ν are illustrated in Figure 9, along with the observed values for the Tonga subduction zone from this study.

5.3. Interpretation of the Tonga Slab Anomaly

Standard thermal models of subduction coupled with reasonable values for the thermal derivatives of seismic velocity provide good fits to the P and S wave data, accounting for both the range and magnitude of the travel time residuals. More importantly, the ratio of thermal derivatives that we infer is consistent with the results of mineral physics experiments. Thus the ν values inferred from both the slab modeling and the residual slope analysis fall within the range expected for thermal perturbations (Figure 9). This lends further credence to the generally accepted notion of slab velocity anomalies being due to decreased temperatures.

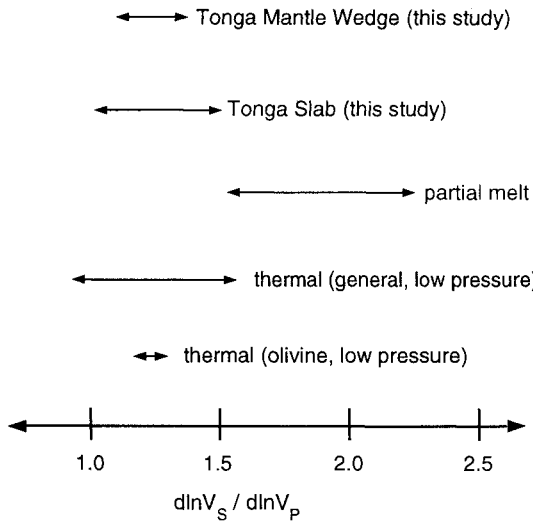

Figure 9. Theoretical estimates of ν for various types of velocity anomalies. References are given in the text. The only types of anomalies that can produce the magnitude, range, and correlation of the observed residuals are partial melting and temperature variations; however, partial melting is ruled out unless theoretical ν_{pm} values overestimate the real Earth value. Both the slab and mantle wedge anomalies are consistent with a thermal perturbation.

5.4. Interpretation of Tonga Mantle Wedge Anomaly

The seismic anomalies beneath the Lau back arc spreading center have frequently been attributed to partial melt [*Aggarwal et al.*, 1972; *Zhao et al.*, 1997]. Partial melt can explain the correlation and magnitude of the velocity anomalies, since a region with only 3% partial melt might produce P wave reductions of 5.4% and S wave reductions of 9.9% for specific melt geometries [*Faul et al.*, 1994]; however, the observed values for ν_{mw} are distinctly lower than what would be expected for the presence of partial melt (Figure 9). Both the residual slope and subduction zone modeling methods suggest a ν of 1.2-1.3 for the mantle wedge region, consistent with the velocity anomaly being primarily due to a temperature variation.

There are thus two possibilities for explaining the nature of the mantle wedge anomaly. The first is that current estimates of ν for partial melt overestimate the real Earth value. The expected partial melt value (ν_{pm}) may be more suspect than the expected thermal value (ν_{thermal}) because the estimates for ν_{thermal} are based on extensive laboratory experiments while estimates of ν_{pm} are based largely on theoretical considerations, owing to the difficulty of conducting laboratory experiments on the effect of partial melt on relative velocity variation. For instance, the calculations of *Mavko* [1980] for ν_{pm} do not take into account the fact that as melt forms in a medium, the remaining solid matrix becomes stiffer as volatiles are extracted, an effect, which besides dampening the magnitude of velocity anomalies generated by partial melt, may affect their relative variation, and thus ν_{pm}, as well.

The second possibility is that the melt which is generated beneath the Lau spreading center is quickly removed from the mantle, and thus the bulk signature of the velocity anomaly is that of a temperature perturbation. This is supported by geodynamical calculations [*Richter and McKenzie*, 1984; *Scott and Stevenson*, 1986] as well as experimental data [*Kohlstedt*, 1992] which suggest that melt is efficiently removed from the rock matrix after formation. Combining the Q values of *Roth et al.* [1999] with calculations on the anelastic amplification of seismic velocity temperature derivatives *Karato* [1993], we find that a temperature increase of 400-600°C can account for the magnitude of the velocity anomalies observed in the mantle wedge.

Such a large temperature increase in the uppermost mantle wedge, where the velocities are slowest, can be accounted for by reduced lithospheric th15100s and mantle upwelling under the Lau spreading center. The fact that the Lau basin is opening at a rate of 13 cm/yr

[*Bevis et al.*, 1995] implies that significant mantle upwelling is occurring beneath the spreading center. Thermal modeling of subduction also suggests that a counterflow is initiated in the mantle wedge, with upwelling in the back arc, and that the diffusion of heat from the mantle wedge into the slab is limited to a small area near the slab-athenosphere boundary [*Kincaid and Sacks*, 1997]. Thus convective heat transfer is more important than conductive heat transfer in the wedge region, especially when the oceanic lithosphere is subducting at a quick rate (as in Tonga), and so the thermal structure in the mantle wedge should be similar to, or even hotter than, that of young oceanic lithosphere.

Figure 10 shows a comparison of a typical conductive lithospheric geotherm [*Turcotte and Schubert*, 1982], representative of the thermal structure for a continental velocity model such as IASP91, a geotherm for old oceanic lithosphere (100 Myr), and a geotherm for young (5 Myr) oceanic lithosphere, as might be expected for the mantle wedge region. Upper and lower bounds (based on volatile content) of the solidus of peridotite are also shown [*Thompson*, 1992]. Figure 10 illustrates that in the shallow upper mantle (20-100 km) there is room for large temperature increases with respect to both ambient continental temperature and the temperature of old oceanic lithosphere, of the order of the 400-600°C required by the data, before the water-saturated peridotite solidus is reached. Furthermore, since it is clear that melt is being produced in the uppermost mantle beneath the Lau spreading center, it follows that the temperature must be several hundred degrees warmer than typical mantle such that the water-saturated peridotite solidus, at the least, is met. As shown in Figure 10, the reduction of T_m with decreasing depth is not significant enough to allow the existence of decompression melting without a large temperature anomaly relative to normal mantle. Thus the large, convection-induced, temperature increase in the mantle wedge region produces the bulk of the seismically observed velocity anomalies, and the effect of partial melt is negligible.

Deeper in the upper mantle (> 100 km), where temperatures beneath the Lau spreading center are expected to be closer to global averages, it may be the presence of volatiles released from the slab that explains the observed low-velocity anomaly. It is well established that the presence of water reduces the solidus curve of peridotite [e.g., *Olaffson and Eggler*, 1983; *Thompson*, 1992], and it has also been proposed that dehydration reactions can occur in subducting oceanic lithosphere to depths of at least 400 km, implying that mantle wedge regions are areas of high volatile content relative to the ambient mantle [*Nolet*, 1994; *Nolet and Zielhuis*, 1994]. If seismic velocity can be approximated as a linear function of homologous temperature, as suggested by *Sato and Sacks* [1989], then the reduction of the melting temperature by the presence of water or other volatiles may affect seismic velocity in a similar manner as an increase

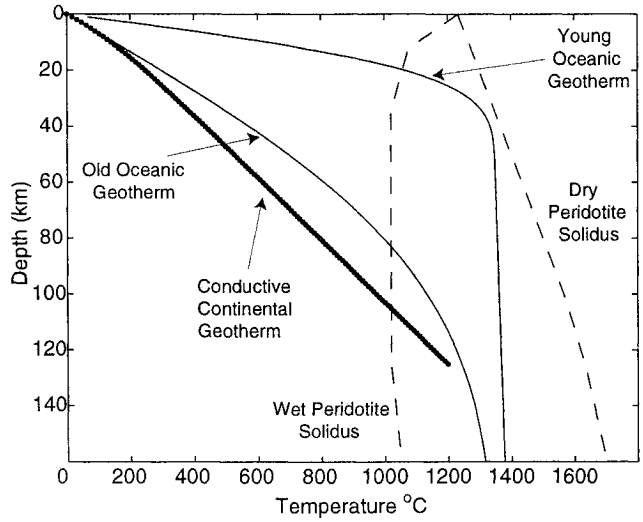

Figure 10. Comparison of continental and oceanic geotherms with solidus curves for peridotite. The continental geotherm is indicated by the dotted line, the oceanic geotherms are indicated by the solid lines, and the solidus curves are indicated by the dashed lines. The continental geotherm is taken from *Turcotte and Schubert* [1982] and is typical for the continental lithosphere that the IASP91 velocity model is based on; the warm oceanic geotherm is constructed for 5 Myr old oceanic lithosphere, assuming a half-space cooling model, and should be appropriate for the actively spreading back arc region; the cold oceanic geotherm is constructed for 100 Myr old lithosphere, again using a half-space cooling model, and illustrates the large variation in temperature which exists for oceanic lithosphere; the peridotite solidi are taken from *Thompson* [1992] and illustrate the influence of volatiles on melting temperature.

in absolute temperature: both types of perturbations weaken the chemical bonds of mantle material. If we assume that

$$V = c_1 \frac{T}{T_m} + c_0, \tag{3}$$

where V is seismic velocity, T is the absolute temperature, T_m is the melting temperature, and c_0 and c_1 are compositionally dependent constants, then to first order

$$\delta V = \frac{c_1}{T_m}\delta T - \frac{c_1 T}{T_m^2}\delta T_m. \tag{4}$$

Thus the magnitude of a velocity change caused by a decrease in T_m is equal to a similar increase in absolute temperature, scaled by the original homologous temperature (T/T_m). Since the homologous temperature is the same for P and S waves, the ν value for changes in melting temperature is the same as for changes in absolute temperature.

If we assume that T_m in the mantle wedge decreases by 300-400°C because of increased volatile content with respect to the ambient mantle and we assume a homologous temperature 0.8, then by (4), this is equivalent to

an absolute temperature increase of 240-320°C. Combining Q values from *Roth et al.* [1999] with temperature derivatives from *Karato* [1993], this temperature anomaly results in 3-5% and 5-7% reductions in P and S wave velocity, respectively. Thus this mechanism can explain the magnitude of the observed velocity anomalies in the deeper part of the mantle wedge. Increased volatile content may contribute somewhat to the reduction of seismic velocities at shallower depths as well, but it is likely that the concentration of volatiles in the shallow mantle wedge has been greatly reduced via melt production and extraction.

6. Conclusions

Two temporary deployments of seismometers in the southwest Pacific have produced a set of high-quality P and S travel times from deep and intermediate events which clearly identify the mantle wedge and slab velocity anomalies of the Tonga subduction zone. Using a standard thermal model of subduction (slab temperatures 500-1000 K colder than the ambient mantle), we find estimates of the temperature derivatives of P and S wave velocity that are consistent with laboratory values determined with rock samples and somewhat smaller than previous seismic estimates and single-crystal laboratory experiments: $dV_p/dT = -0.23$ $\mathrm{ms^{-1}K^{-1}}$ and $dV_s/dT = -0.20$ $\mathrm{ms^{-1}K^{-1}}$. Standard error estimates associated with arrival time uncertainty are significantly smaller than those due to model biases which give a range of accepted values of -0.2 to -0.4 $\mathrm{ms^{-1}K^{-1}}$ for P waves. The ratio of values is more stable, however, and falls within the range predicted by mineral physics experiments on the effect of temperature on seismic velocity. A linear regression of S and P residuals yields an independent estimate of the relative velocity variation of the Tonga slab that is somewhat smaller ($\nu \sim 1.1$-1.2 as opposed to $\nu \sim 1.5$) but is still consistent with the bulk of the slab anomaly being due to a temperature perturbation.

For the mantle wedge velocity anomaly, both the residual slope analysis and the finite difference travel time modeling yield ν values of 1.2-1.3. Errors associated with location uncertainty and model assumptions are unable to increase the inferred values above 1.5, indicating that ν is not distinctly different in the mantle wedge than in the slab. These ν values are smaller than what is theoretically predicted by models of partial melt but agree with thermal predictions based on laboratory experiments. Accounting for the anelastic amplification of temperature derivatives of seismic velocity, a 400-600°C temperature anomaly is required to generate the observed amplitude of the velocity reductions in the upper (<100 km) part of the mantle wedge. Such a large temperature increase with respect to the ambient mantle is possible because of the convective upwelling in Lau back arc basin. The thermal structure of the region should be closer to that of young oceanic lithosphere, and thus several hundred degrees warmer, than that of typical continental lithosphere. In the deeper part of the mantle wedge (100-400 km), it is likely that the low-magnitude velocity reductions are caused by increased volatile content with respect to normal mantle. Volatiles can significantly decrease the melting temperature and thus generate velocity anomalies with a thermal signature.

Acknowledgments. The SPASE project used instruments and equipment from the PASSCAL program of the Incorporated Research Institutions in Seismology (IRIS), a facilities program of the National Science Foundation (NSF). We would like to thank several people who provided significant assistance in collecting data used in this study, both on the SPASE project and the Lau Basin OBS deployment: Mike Bevis, Wayne Crawford, Kitione Draunidalo, Sharon Esher, Tavita Fatai, Paul Friberg, Saimone Helu, Mark McDonald, Erich Roth, Allan Sauter, Patrick Shore, and Lasarusa Veutibau. We also would like to thank John Vidale and John Hole for providing their finite difference travel time code and advice on using it, Yingbiao Xu for providing his S wave model of the Lau basin prior to publication, and Erich Roth for providing his attenuation model prior to publication. We thank Rob van der Hilst, Emile Okal, and an anonymous referee for critically reviewing the manuscript. This work was supported by NSF grants EAR9219675, OCE9314446, and EAR9614502; CSEDI grant EAR9712311; and a Carl Tolman fellowship.

References

Aggarwal, Y. P., and M. Barazangi, P and S travel times in the Tonga-Fiji region: A zone of low velocity in the uppermost mantle behind the Tonga Island Arc, *J. Geophys. Res., 77*, 6427-6434, 1972.

Agnon, A., M. S. T. Bukowinski, δ_s at high pressure and $\mathrm{dln}V_s/\mathrm{dln}V_p$ in the lower mantle, *Geophys. Res. Lett., 17*, 1149-1152, 1990.

Anderson, D. L., Thermally induced phase changes, lateral heterogeneity of the mantle, continental roots, and deep slab anomalies, *J. Geophys. Res., 92*, 13968-13980, 1987.

Anderson, O. L., D. Isaak, and H. Oda, High-temperature elastic constant data on minerals relevant to geophysics, *Rev. Geophys., 30*, 57-90, 1992.

Bevis, M., F. W. Taylor, B. E. Schutz, J. Recy, B. L. Isacks, S. Helu, R. Singh, E. Kendrick, J. Stowell, B. Taylor, and S. Calmant, Geodetic observations of a very rapid convergence and back-arc extension at the Tonga Arc, *Nature, 374*, 249-251, 1995.

Bokelmann, G. H. R., and P. G. Silver, The Caribbean anomaly: Short-wavelength lateral heterogeneity in the lower mantle, *Geophys. Res. Lett., 20*, 1131-1134, 1993.

Christensen, N. I., Compressional wave velocity in rocks at high temperatures and pressures: Critical thermal gradients, and crustal low-velocity zones, *J. Geophys. Res., 84*, 6849-6857, 1979.

Creager, K. C., and T. Jordan, Slab penetration into the lower mantle beneath the Mariana and other island arcs of the northwest Pacific, *J. Geophys. Res., 91* , 3573-3589, 1986.

Doyle, H. A., and A. L. Hales, An analysis of the travel times of S waves to North American stations, in the distance range 28°to 82°, *Bull. Seismol. Soc. Am., 57*, 761-771, 1967.

Duffy, T. S., and T. J. Ahrens, Sound velocities at high pressure and temperature and their geophysical implications, *J. Geophys. Res., 97*, 4503-4520, 1992.

Dziewonski, A. M., and D. L. Anderson, Preliminary reference Earth model, *Phys. Earth Planet. Inter., 25*, 297-356, 1981.

Dziewonski, A. M., and J. H. Woodhouse, Global images of the Earth's interior, *Science, 236*, 37-48, 1987.

Faul, U. H., D. R. Toomey, and H. S. Waff, Intergranular basaltic melt is distributed in thin, elongated inclusions, *Geophys. Res. Lett., 21*, 29-32, 1994.

Fischer, K. M., and D. A. Wiens, The depth distribution of mantle anisotropy beneath the Tonga subduction zone, *Earth Planet. Sci. Lett., 142*, 253-260, 1996.

Fischer, K. M., K. C. Creager, and T. H. Jordan, Mapping the Tonga slab, *J. Geophys. Res., 96*, 14403-14427, 1991.

Giardini, D., X. D. Li, and J. Woodhouse, Three-dimensional structure of the Earth from splitting in free-oscillation data, *Nature, 325*, 405-411, 1987.

Hales, A. L., A look at the mantle, *Geotimes, 9*, 9-13, 1964.

Hales, A. L., and H. A. Doyle, P and S travel time anomalies and their interpretation, *Geophys. J. R. Astron. Soc., 13*, 403-415, 1967.

Hales, A. L. and E. Herrin, Travel times of seismic waves, in *The Nature of the Solid Earth* , edited by E. C. Robinson, J. F. Hays, and L. Knopoff, pp. 172-215, McGraw-Hill, New York, 1972.

Hales, A. L., and J. L. Roberts, The travel times of S and *SKS*, *Bull. Seismol. Soc. Am., 60*, 461-489, 1970.

Holbrook, W. S., W. D. Mooney, and N. I. Christensen, The seismic velocity structure of the deep continental crust, in *Continental Lower Crust*, edited by D. M. Fountain, R. Arculus, and R. W. Kay, pp. 1-43, Elsevier, New York, 1992.

Hole, J. A., and B. C. Zelt, 3-D finite-difference reflection travel times, *Geophys. J. Int., 121*, 427-434, 1995.

Isaak, D. G., O. L. Anderson, and R. E. Cohn, The relationship between shear and compressional velocities at high pressures: Reconciliation of seismic tomography and mineral physics, *Geophys. Res. Lett., 19*, 741-744, 1992.

Jeffreys, H., and K. Singh, Comparison of station errors in seismology, *Geophys. J. R. Astron. Soc., 32*, 423-437, 1973.

Karato, S., Importance of anelasticity in the interpretation of seismic tomography, *Geophys. Res. Lett., 20*, 1623-1626, 1993.

Kennett, B. L. N., and E. R. Engdahl, Traveltimes for global earthquake location and phase identification, *Geophys. J. Int., 105*, 429-465, 1991.

Kennett, B. L. N., S. Widiyantoro, and R. D. van der Hilst, Joint seismic tomography for bulk sound and shear wave speed in the Earth's mantle, *J. Geophys. Res., 103*, 12469-12493, 1998.

Kern, H., and A. Richter, Temperature derivatives of compressional and shear wave velocities in crustal and mantle rocks at 6 kbar confining pressure, *J. Geophys., 49*, 47-56, 1981.

Kincaid C., and I. S. Sacks, Thermal and dynamical evolution of the upper mantle in subduction zones, *J. Geophys. Res., 102*, 12295-12315, 1997.

Knoche, R., S. L. Webb, and D. C. Rubie, Experimental determination of acoustic wave velocities at Earth mantle conditions using a multianvil press, *Phys. Chem. Earth, 22*, 125-130, 1997.

Koch, M., Bootstrap inversion for vertical and lateral variations of the S wave structure and the vp/vs-ratio from shallow earthquakes in the Rhinegraben seismic zone, Germany, *Tectonophysics, 210*, 91-115, 1992.

Kohlstedt, D. L., Structure, rheology, and permeability of partially molten rocks at low melt fraction, in *Mantle Flow and Melt Generation at Mid-Ocean Ridges, Geophys. Monog. Ser.*, vol. 71, edited by J. P. Morgan, D. K. Blackmann, and J. M. Sinton, pp. 103-122, AGU, Washington, D. C., 1992.

Koper, K. D., D. A. Wiens, L. M. Dorman, J. A. Hildebrand, and S. C. Webb, Modeling the Tonga slab: Can travel time data resolve a metastable olivine wedge?, *J. Geophys. Res., 103*, 30079-30100, 1998.

Li, X. D., D. Giardini, and J. H. Woodhouse, The relative amplitudes of mantle heterogeneity in P velocity, S velocity and density from free-oscillation data, *Geophys. J. Int., 105*, 649-657, 1991.

Mavko, G. M., Velocity and attenuation in partially molten rocks, *J. Geophys. Res., 85*, 5173-5189, 1980.

McNutt, M. K., and A. V. Judge, The superswell and mantle dynamics beneath the South Pacific, *Science, 248*, 969-975, 1990.

Nolet, G., Seismic evidence for the occurrence of volatiles below 200 km depth in the Earth, in *Volatiles in the Earth and Solar System, AIP Conf. Proc., 341*, edited by K. A. Farley, 22-32, 1994.

Nolet, G., and A. Zielhius, Low S velocities under the Tornquist-Teissetre zone: Evidence for water injection into the transition zone by subduction, *J. Geophys. Res., 99*, 15813-15820, 1994.

Olafsson, M., and D. H. Eggler, Phase relations of amphibole, amphibole-carbonate, and phlogopite-carbonate peridotite: Petrologic constraints on the athenosphere, *Earth Planet. Sci. Lett., 64*, 305-315, 1983.

Richter, F. M., and D. McKenzie, Dynamical models for melt segregation from a deformable matrix, *J. Geol., 92*, 729-740, 1984.

Robertson, G. S., and J. H. Woodhouse, Ratio of relative S to P velocity heterogeneity in the lower mantle, *J. Geophys. Res., 100*, 20041-20052, 1996.

Robertson, G. S., and J. H. Woodhouse, Comparison of P and S station corrections and their relationship to upper mantle structure, *J. Geophys. Res., 102*, 27355-27366, 1997.

Romanowicz, B., and M. Cara, Reconsideration of the relations between S and P station anomalies in North America, *Geophys. Res. Lett., 7*, 417-420, 1980.

Roth, E. G., D. A. Wiens, L. M. Dorman, J. Hildebrand, and S. C. Webb, Seismic attenuation tomography of the Tonga-Fiji region using phase pair methods, *J. Geophys. Res., 104*, 4795-4809, 1999.

Sato, H., and I. S. Sacks, Anelasticity and thermal structure of the oceanic upper mantle: Temperature calibration with heat flow data, *J. Geophys. Res., 94*, 5705-5715, 1989.

Scott, D. R., and D. J. Stevenson, Magma ascent by porous flow, *J. Geophys. Res., 91*, 9283-9296, 1986.

Schwartz, S. Y., T. Lay, and S. P. Grand, Seismic imaging of subducted slabs: Trade-offs with deep path and near-receiver effects, *Geophys. Res. Lett., 18*, 1265-1268, 1991.

Sleep, N. H., Teleseismic P wave transmission through slabs, *Bull. Seismol. Soc. Am., 63*, 1349-1373, 1973.

Smith, G. P., D. A. Wiens, L. M. Dorman, S. C. Webb, and K. M. Fischer, Azimuthal anisotropy beneath the Lau Basin: Observations of shear wave splitting from local earthquakes at ocean bottom seismometers, *Eos Trans. AGU, 79*(45), Fall Meet. Suppl., F637, 1998.

Souriau, A., and J. H. Woodhouse, A worldwide comparison of predicted S wave delays from a three-dimensional upper mantle model with P wave station cor15103s, *Phys. Earth Planet. Inter., 39*, 75-88, 1985.

Stein, C. A., and S. Stein, A model for the global variation in oceanic depth and heat flow with lithospheric age, *Nature, 359*, 123-129, 1992.

Su, W., and A. M. Dziewonski, Simultaneous inversion for 3-D variations in shear and bulk velocity in the mantle, *Phys. Earth Planet. Inter., 100*, 135-156, 1997.

Suyehiro, K., and I. S. Sacks, *P* and *S* wave velocity anomalies associated with the subducting lithosphere determined from travel-time residuals in the Japan region, *Bull. Seismol. Soc. Am., 69*, 97-114, 1979.

Taylor, B., K. Zellmer, F. Martinez, and A. Goodliffe, Seafloor spreading in the Lau backarc basin, *Earth Planet. Sci. Lett., 144*, 35-40, 1996.

Thompson, A. B., Water in the Earth's upper mantle, *Nature, 328*, 295-302, 1992.

Toksöz, M. N., N. H. Sleep, and A. T. Smith, Evolution of the downgoing lithosphere and mechanisms of deep focus earthquakes, *Geophys. J. R. Astron. Soc., 35*, 285-310, 1973.

Toomey, D. R., W. S. D. Wilcock, S. C. Solomon, W. C. Hammond, and J. A. Orcutt, Mantle seismic structure beneath the MELT region of the East Pacific Rise from *P* and *S* wave tomography, *Science, 280*, 1224-1227, 1998.

Turcotte, D. L., and G. Schubert, *Geodynamics Applications of Continuum Physics to Geological Problems*, 148 pp., John Wiley, New York, 1982.

Vidale, J. E., Finite-difference calculation of travel times in three dimensions, *Geophysics, 55*, 521-526, 1990.

Wickens, A. J., and G. G. R. Buchbinder, *S* wave residuals in Canada, *Bull. Seismol. Soc. Am., 70*, 809-822, 1980.

Wiens, D. A., P. J. Shore, J. J. McGuire, E. Roth, M. G. Bevis, and K. Draunidalo, Southwest Pacific seismic experiment *IRIS Newsl., 14*, 1-4, 1995.

Woodhouse, J. H., and A. M. Dziewonski, Mapping the upper mantle: Three-dimensional modeling of earth structure by inversion of seismic waveform, *J. Geophys. Res., 89*, 5953-5986, 1984.

Xu, Y., and D. A. Wiens, Upper mantle structure of the southwest Pacific from regional waveform inversion, *J. Geophys. Res., 102*, 27439-27451, 1997.

York, D., Least-squares fitting of a straight line, *Can. J. Phys., 44*, 1079-1086, 1966.

Zandt, G., and C. J. Ammon, Continental crust composition constrained by measurements of crustal Poisson's ratio, *Nature, 374*, 152-154, 1995.

Zhao, D., H. Kanamori, H. Negishi, and D. A. Wiens, Tomography of the source area of the 1995 Kobe earthquake: Evidence for fluids at the hypocenter, *Science, 274*, 1891-1894, 1996.

Zhao, D., Y. Xu, D. A. Wiens, L. Dorman, J. Hildebrand, and S. Webb, Depth extent of the Lau back-arc spreading center and its relation to subduction processes, *Science, 278*, 254-257, 1997.

Zhou, H.-W., D. L. Anderson, and R. W. Clayton, Modeling of residual spheres for subduction zone earthquakes, 1, Apparent slab penetration signatures in the NW Pacific caused by deep diffuse mantle anomalies, *J. Geophys. Res., 95*, 6799-6827, 1990.

L. Dorman, J. Hildebrand, and S. Webb, Scripps Institution of Oceanography, University of California, San Diego, La Jolla, CA 92093. (ldorman@ucsd.edu; jhildebrand@ucsd.edu; scweb@ucsd.edu)

K. D. Koper, Department of Geosciences, University of Arizona, Gould-Simpson 208, Tuscon, AZ 85721. (kkoper@geo.arizona.edu)

D. A. Wiens, Department of Earth and Planetary Science, Washington University, One Brookings Drive, CB 1169, St. Louis, MO 63130-4899. (doug@mantle.wustl.edu)

(Received June 17, 1998; revised January 29, 1999; accepted March 30, 1999.)